Microscopic Mechanisms of Self-Compensation in Si δ-Doped GaAs

S. Modesti,* R. Duca,* P. Finetti, G. Ceballos, M. Piccin,* S. Rubini, and A. Franciosi*

Laboratorio Nazionale TASC-INFM, Area Science Park, S.S. 14, Km. 163.5, I-34012 Trieste, Italy

(Received 6 October 2003; published 27 February 2004)

We combined systematic cross-sectional scanning tunneling microscopy and spectroscopy investigations with Hall measurements on single Si δ-doped layers, as well as Si δ-doped superlattices in GaAs. We found that Si self-compensation involves nucleation and growth of electrically neutral Si precipitates at the expense of the conventional donor Si phase.

DOI: 10.1103/PhysRevLett.92.086104 PACS numbers: 68.55.Ln, 61.72.Ss, 68.37.Ef, 85.40.Ry

Doping plays a fundamental role in determining the properties of semiconductors, and limitations in doping technology currently limit the performance of many optoelectronic and high-speed devices. For Si-doped GaAs, the observed limit in the maximum free-electron density achievable with increasing Si concentration has been associated with a variety of mechanisms, including autocompensation (self-compensation) of Si_{Ga} donors by Si_{As} acceptors, formation of Si pairs, Si clusters, complexes of Si atoms with native defects, and existence of a nonhydrogenic Si level resonant with the conduction band [1–3]. Establishing a microscopic picture of dopant compensation will require careful control of the material fabrication parameters and complementing the traditional transport and optical methods with atomic resolution imaging of point defects [4–7] within *statistically significant* portions of the material.

We focus here on self-compensation in Si δ-doped GaAs. Deposition of submonolayer coverages of impurities during a semiconductor growth interruption is used to fabricate high-density, two-dimensional (2D) electron or hole gases in a variety of devices [8–10]. We selected the deposition parameters most commonly used in current GaAs technology and determined the microscopic events that give rise to self-compensation using cross-sectional scanning tunneling microscopy (XSTM) and spectroscopy (XSTS) data supported by evidence from Hall calibration samples.

All structures were fabricated on GaAs(001) wafers by molecular beam epitaxy (MBE), with growth temperature monitored by means of an infrared pyrometer. Following thermal removal of the native oxide, a 0.5 μm thick GaAs(001) 2×4 buffer layer was grown at 600 °C with a As/Ga beam pressure ratio of 15 and an overall GaAs growth rate of 1 μm/h, i.e., 0.98 Ga-As bilayers per second, or (6.25×10^{14} Ga atoms $+6.25 \times 10^{14}$ As atoms) $\mathrm{cm}^{-2}\,\mathrm{s}^{-1}$. Deposition of the Si layers was also performed at 600 °C at a rate of 2×10^{-3} monolayers per second (with 1 monolayer = 1 ML = 6.25×10^{14} atoms cm^{-2}), interrupting the growth of the GaAs host crystal by closing the Ga shutter and opening the Si shutter while leaving the As shutter open. Silicon surface densities n_s examined ranged from 6.25×10^{12} cm^{-2} to 1.25×10^{15} cm^{-2} (i.e., from 0.01 to 2 ML) within each δ-doped layer. To cap the structure, a 100 nm-thick GaAs layer was grown in the same conditions used for the buffer.

Samples for XSTM and XSTS analysis were comprised of ten δ-doped layers spaced by 50 nm GaAs barriers and included n-doped buffer and cap layers (1.6×10^{17} Si donors cm^{-3}, 500 nm-thick) and an n^+ substrate (0.8–2.1×10^{18} Si donors cm^{-3}). Samples for Hall measurements were grown immediately after the XSTM/XSTS samples with identical structure, but for the undoped buffer and cap layers and semi-insulating substrates (substrate resistivity 1–$4 \times 10^7\ \Omega\,\mathrm{cm}$). The sheet carrier density at room temperature was determined on such samples by means of Hall measurements in the van der Pauw geometry. To simulate the effect of the different times spent at the growth temperature by the different δ-doped layer within the superlattice, we also fabricated Hall calibration samples with single δ-doped layers, 500 nm-thick undoped buffer and cap layers, and semi-insulating substrates, and subjected them to postgrowth anneals for 2 h at 600 °C in the MBE chamber under As flux.

The free-electron density obtained from the Hall measurements is summarized as a function of n_s (from flux calibrations) in Fig. 1 for the single δ-doped layers (open squares). No data correction for depletion effects was required, as indicated by the negligible differences observed in the measured free-carrier concentration for test samples containing thin (100 nm) as opposed to thick (500 nm) cap layers. Full electrical activation of the Si donors was observed for n_s below 0.06 ML. At higher Si coverages self-compensation yielded a nearly coverage-independent sheet carrier density of 1.5–2.0×10^{13} cm^{-2}. Correspondingly, the measured electron mobility (not shown) decreased as expected with increasing sheet carrier density to saturate at a nearly coverage-independent mobility of 6–8×10^2 $\mathrm{cm}^2\,\mathrm{V}^{-1}\,\mathrm{s}^{-1}$ for n_s above 0.06 ML. Upon annealing the single δ-doped layers (open circles), the electron density (see Fig. 1) was seen to *decrease* by a factor of 2 to 3 in the compensated samples, while it remained unchanged, within experimental uncertainty, in all of the samples below the onset of

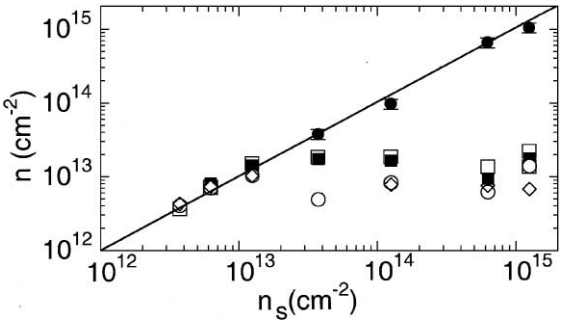

FIG. 1. Hall-derived free-electron density per period in Si δ-doped GaAs samples. We compare results for single δ-doped layers as grown (open squares), after a 2 h postgrowth anneal (open circles), and for ten period Si δ-doping superlattices (open diamonds). The solid line denotes the Si surface density per period n_s (from Si flux calibrations). Solid symbols show the number of Si_{Ga} donors (solid squares) and Si atoms within neutral Si precipitates (solid circles) as derived from XSTM studies of the topmost (last-deposited) superlattice period.

self-compensation. This remarkable result is *per se* a strong indication that self-compensation may involve sequential nucleation and growth stages, and a kinetically limited transition between different silicon phases. Annealing yielded, instead, comparatively little change in the measured electron mobility. For comparison, we included in Fig. 1 Hall results for the superlattice samples. The free-electron density per period in such samples (open diamonds) is compellingly similar to that observed in the annealed single δ-doped layers (open circles) and in good quantitative agreement with what has been reported by other authors for similar growth conditions [10,11]. Because of the growth times involved, results for as-grown single δ-doped samples (open squares) are representative of the situation found in the last-deposited periods within the superlattices, while the annealed single δ-doped samples (open circles) are more similar to the first-deposited periods, which have remained at the growth temperature 1.5 to 3.5 h (for $n_s = 0.2$ to 2 ML).

Scanning tunneling microscopy (STM) measurements were performed in ultrahigh vacuum with W tips. The 0.1 mm thick wafers were cleaved *in situ* immediately prior to image acquisition to yield atomically flat, electronically unpinned {110} surfaces normal to the [001] growth direction. The area sampled with atomic resolution was larger than 2×10^4 nm^2 for each value of n_s.

Representative constant-current STM micrographs of the (110) cleavage surface intersecting the Si layers are shown in Fig. 2. The intersection line is marked by vertical arrows. The Si_{Ga}donors in the first 4–5 atomic layers below the surface give rise to circular bright hillocks ~2 nm wide both at negative and positive sample bias V_b (-1.4 V $> V_b > -2.5$ V or $1.7 < V_b < 3$ V) [12]. The dark areas at negative V_b are caused by surface Ga vacancies (V_{Ga}). Their density grows with time in the heavily n-doped regions. For some tip configurations, a bright narrow maximum—corresponding to two adjacent As atoms—appears at the center of the dark V_{Ga} induced regions [1].

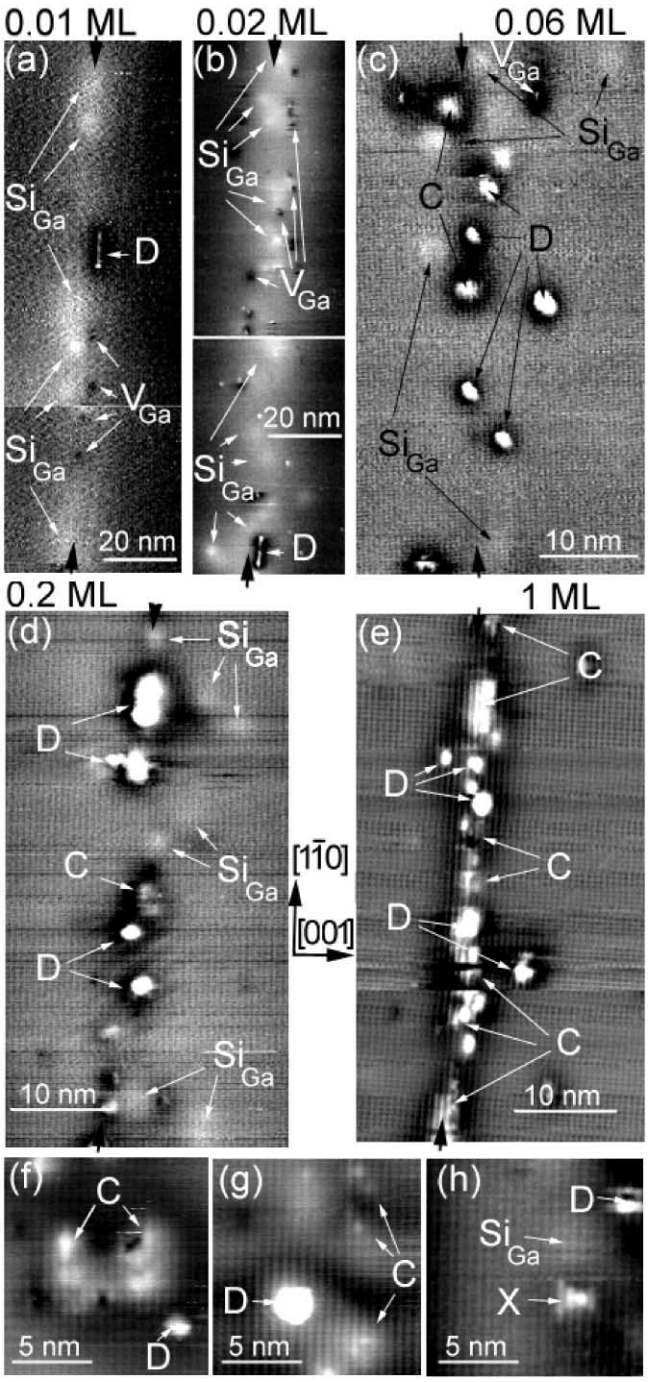

FIG. 2. (a)–(e) XSTM topographic images of the intersections of Si layers in GaAs with the (110) cleavage surface for n_s ranging from 0.02 to 1 ML. Substitutional Si donors Si_{Ga}, surface gallium vacancies V_{Ga}, and Si precipitates C are visible. (f) and (g) images of C defects at 0.2 ML. (h) Image of a minority unidentified defect X. The tunneling current was 0.2 nA , V_b was 1.8 V for (a) and (b) and between -1.5 and -1.8 V for (c)–(h).

Si_{Ga} atoms within the first atomic layer induce features resembling those caused by V_{Ga} defects at $V_b < 0$ [1], and

are more difficult to identify as compared to Si_{Ga} in deeper layers. For this reason, the analysis that follows for Si_{Ga} is based solely on the data obtained from the deeper layers. Cleavage defects (D) 0.2 nm high, i.e., missing or added rows of atoms, are frequent near the δ-doped layers. These surface features are a result of the cleavage process in areas locally stressed by the high Si concentration and do not correspond to bulk defects. Their density increases with that of Si. At $n_s = 0.01$ ML, the donors are confined within 2 nm from the original (001) plane; at $n_s = 0.02$ ML their distribution along the [001] growth direction broadens to ~5 nm. Up to this value of n_s, the observed defects are Si_{Ga}, V_{Ga}, and cleavage defects D.

Above the onset of self-compensation (see Fig. 1), i.e., for $n_s \geq 0.06$ ML, new characteristic features appear. Most of them are imaged as asymmetric, irregular bright areas surrounded by a dark halo at negative V_b, and as dark regions at positive V_b. They are denoted by C in the images. These defects are on the average ~1 nm wide for $n_s = 0.06$ ML and ~2 nm wide for $n_s = 0.02$ ML [see Figs. 2(f) and 2(g)]. Because of their irregular shape and their dependence on V_b, they can be easily discriminated from the circular features induced by Si_{Ga} donors and any hypothetical Si_{As} acceptor [1]. Their linear density along the $[1\bar{1}0]$ direction is $(3 \pm 1) \times 10^5$ cm^{-1} at $n_s = 0.06$ ML, and increases to $(1.0 \pm 0.3) \times 10^6$ cm^{-1} at $n_s = 0.02$ ML. At $n_s = 1$ and 2 ML, they form a nearly continuous strip 0.5–3 nm wide [13].

The contrast of this strip depends on V_b and it is strongly attenuated or inverted for $V_b > 0$. Therefore it cannot be formed by single Si_{Ga} donors. Isolated Si_{Ga} donors are still present and they are spread out within 10 nm from the bright strip. Since the bright regions have sharp boundaries, they are not caused by the potential of charged subsurface structures. If we assume that each bright unit cell is associated with a surface Si atom, the integrated densities observed in the different samples correspond to 0.06, 0.15, 1.1, and 1.8 ML of Si. Such values, denoted by solid circles in Fig. 1, are very close to the total density of Si atoms expected from flux calibrations (solid line) in the high-coverage range.

The distributions of the Si_{Ga} donors and of the bright regions C along the [001] growth direction are shown in Fig. 3 as a function of n_s for the topmost (last-deposited) superlattice layers, kept at the growth temperature for the same amount of time, i.e., 2000 s, for all samples. The width of the Si_{Ga}distribution increases from 2 to 9 nm as n_s is increased from 0.01 to 0.06 ML, and then decreases, remaining roughly proportional to the Si_{Ga} density (see below). The center of the donor distribution shifts in the growth direction by 2 up to 5 nm for increasing n_s, relative to the mean position of the C regions. For any given value of n_s, the donor distributions were also found (not shown) to broaden in comparing the last- and first-deposited layers within the superlattice, reflecting the increasing time at the growth temperature.

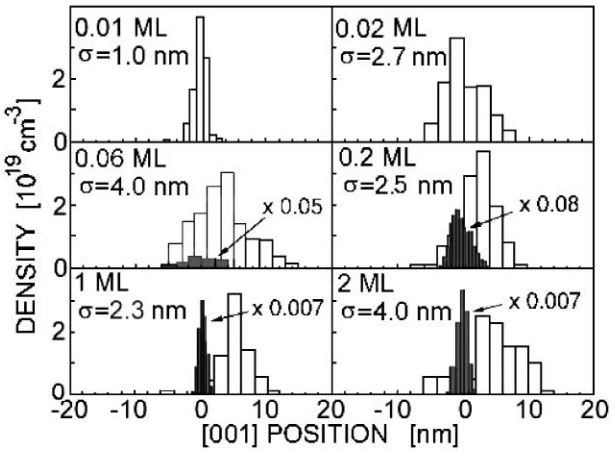

FIG. 3. Distribution of the density of the Si_{Ga} donors (open bars) and of the Si atoms in the C regions (solid bars) along the [001] growth direction. The origin is the center of the Si distribution within the C regions.

We produced XSTM determinations of the density of Si donors from the observed density of Si_{Ga}. We assumed a sampling depth of 4.5 ± 0.5 atomic layers [12] at a donor concentration of 2×10^{19} cm^{-3} and a dependence of the sampling depth on the charged dopant density equal to that reported in Ref. [7]. Such a dependence was verified in the data for our uncompensated samples. Figure 1 clearly shows that the XSTM-derived values (solid squares) are in remarkable quantitative agreement with those obtained from the Hall calibration samples (open squares). Therefore, throughout the n_s range examined, the Si_{Ga} ions and the Si atoms within the precipitates observed by XSTM account for the total Si coverage, as determined from flux calibrations.

Using the XSTM-determined Si donor distribution for the top (Fig. 3) and bottom (not shown) superlattice periods and correcting for the density dependence of the XSTM sampling depth, we obtain a *decrease* in the number of charged impurities with postgrowth annealing by up to a factor of 2 (for the 2 ML sample) in the self-compensated samples. The trend is therefore that expected from the Hall calibration data in Fig. 1 (open squares versus open circles and diamonds), although quantitative determinations of this effect by STM carry a substantially higher experimental uncertainty.

The good agreement of XSTM and Hall results in Fig. 1 lends strong independent support to our XSTM-derived statistics. The density of features other than Si_{Ga}, V_{Ga}, D, and C observed by XSTM amounted to less than 15% of the Si_{Ga} donor density for $n_s < 2$ ML. Such minority defects included contaminations from residual gases and from the STM tip, features compatible with those expected for Si_{As} acceptors [1], and some unidentified Si defects. A typical example of this last class—observed for $n_s \geq 0.06$ ML—is shown in Fig. 2(h) [14].

Because individual Si_{Ga} donors and Si atoms in the precipitates were the only Si phases statistically significant in our samples, the Si precipitates had to be globally

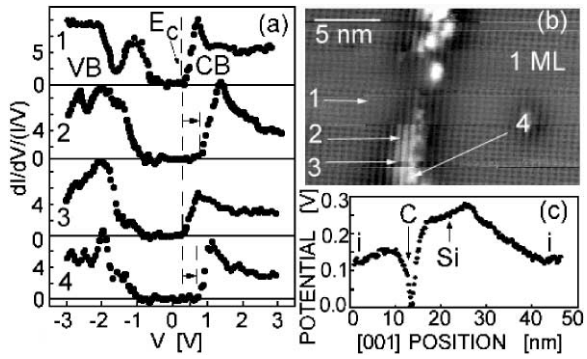

FIG. 4. (a) Tunneling spectra measured close to and in the C region shown in (b). The peak at 1.5 V in spectrum 1 is caused by tunneling of the free carriers in the conduction band CB within the *n*-doped region. (c) potential measured along the [001] direction across a 1 ML-thick Si region. The maximum is in the region of the Si_{Ga} donors; the sharp minimum is caused by the Si-rich layer C; the broad minima correspond to the intrinsic regions on either side of the Si layer.

neutral within the GaAs bulk to explain the observed saturation in the free-carrier density for $n_s \geq 0.06$ ML. XSTS can be used to probe the electronic structure of the precipitates, but only at the cleaved surface. XSTS data acquired near and within the bright regions *C* (Fig. 4) show that the conduction and the valence bands in the bright regions rise in energy by up to 0.5 eV as compared to the neighboring *n*-type regions; i.e., the surface Fermi level is pinned near midgap. This effect was also observed by measuring the local electrostatic potential with the method described in Ref. [15]. A plot of the potential measured along the [001] growth direction and averaged along $[1\bar{1}0]$ [Fig. 4(c)] shows a broad maximum in the region occupied by the Si_{Ga} donors and a narrow 0.2 V deep minimum in the region of the extended defects.

The behavior illustrated in Fig. 4 is consistent with that expected for cleaved Si inclusions in GaAs. While atomically flat GaAs(110) surfaces are known to be electronically unpinned, localized states near midgap have been observed for Si(110) surfaces [16].

Together the Hall and XSTM/XSTS results provide a compelling picture of self-compensation in Si δ-doped GaAs. Below the onset of self-compensation only a gas of highly mobile Si_{Ga} donors is observed, with a spatial distribution that broadens with increasing time at the growth temperature and gradually shifts toward the surface as a result of the combined effect of Coulomb-repulsion enhanced diffusion [17] and partial surface riding [7]. In this regime, postgrowth annealing does not change the free-carrier density, just its spatial distribution. Above the onset of self-compensation, nucleation and growth of Si precipitates near the nominal position of the Si δ-doped layers gradually involves an increasing fraction of the Si atoms, giving rise to a narrow distribution of majority Si (99% at 1–2 ML) in a neutral Si phase, superimposed to the broad, asymmetric distribution of the highly mobile Si_{Ga} donors. In this regime, postgrowth annealing may change the relative abundance of the two Si phases, with the Si precipitates gradually growing at the expense of the donor gas [18].

This work was supported, in part, by INFM under the Progetto di Ricerca Avanzato XSTMS and under Project 5A of the Cluster 26 Program on Advanced Materials.

*Also with Dipartimento di Fisica, Universitá di Trieste, Trieste, Italy.

[1] C. Domke *et al.*, Phys. Rev. B **54**, 10 288 (1996); C. Domke, Ph. Ebert, and K. Urban, Surf. Sci. **415,** 285 (1998), and references therein.
[2] S. Schuppler *et al.*, Phys. Rev. B **51**, 10 527 (1995).
[3] T. N. Theis, P. M. Mooney, and S. L. Wright, Phys. Rev. Lett. **60**, 361 (1988).
[4] R. M. Feenstra, J. M. Woodall, and G. D. Pettit, Phys. Rev. Lett. **71**, 1176 (1993).
[5] J. Gebauer *et al.*, Phys. Rev. Lett. **78**, 3334 (1997).
[6] B. Grandidier *et al.*, Appl. Phys. Lett. **72**, 2454 (1998).
[7] M. B. Johnson *et al.*, Phys. Rev. Lett. **75**, 1606 (1995).
[8] E. F. Schubert, *Doping in II-V Semiconductors* (Cambridge University Press, Cambridge, England, 1993).
[9] M. J. Ashwin *et al.*, J. Appl. Phys. **73**, 633 (1993).
[10] M. Moreno *et al.*, Phys. Rev. B **58**, 13 767 (1998). See, in particular, Fig. 8 and references therein.
[11] K. Kohler, P. Ganser, and M. Maier, J. Cryst. Growth **127**, 720 (1993).
[12] J. F. Zheng *et al.*, Phys. Rev. Lett. **72**, 1490 (1994).
[13] E. Carlino *et al.*, Appl. Phys. Lett. **83**, 662 (2003).
[14] Previous XSTM studies of bulk, heavily doped, seed-grown GaAs reported features attributed to a variety of defect complexes [1] that are not observed in a statistically significant number in the present study of state-of-the-art MBE material. Domke *et al.* did report features due to Si clusters, but we caution the reader that the appearance and bias dependence of such features are inconsistent with those reported here, and consistent, instead, with cleavage defects *D* consisting of missing rows of atoms.
[15] S. Modesti *et al.*, Appl. Phys. Lett. **82**, 1932 (2003).
[16] R. M. Feenstra, M. A. Lutz, and J. O. Chu, Surf. Sci. **328**, 215 (1995).
[17] E. F. Schubert *et al.*, Phys. Rev. B **46**, 15 078 (1992).
[18] The electron mobility decrease with increasing sheet carrier density observed below the onset of self-compensation is consistent with the expected relevance of the ionized impurity scattering rate in our samples, and the observed saturation in electron mobility above the onset is in qualitative agreement with the neutral character of the Si precipitates. The effect of annealing on the electron mobility is more difficult to predict in view of the contrasting effects of annealing on the donor spatial distribution, free-electron sheet carrier density, and Si-induced local strain in samples that are intrinsically anisotropic.